

COUPLED POPULATION BALANCE AND CFD MODEL FOR A CONTINUOUS GIBBSITE CRYSTALLISER

Alex R. HEATH¹ and Iztok LIVK²

¹Parker Cooperative Research Centre for Integrated Hydrometallurgy Solutions
 (CSIRO Minerals) Clayton, Victoria 3169, AUSTRALIA

²Parker Cooperative Research Centre for Integrated Hydrometallurgy Solutions
 (CSIRO Minerals) Waterford, WA 6152, AUSTRALIA

ABSTRACT

A combined population balance (PB) and CFD model was developed to model the behaviour of a continuous stirred tank gibbsite precipitator. The model is 2-phase Eulerian-Eulerian with the population balance particle size groups modelled with a series of solid-phase scalar transport equations. The population balance kernels describe the birth, death, and growth rate of the crystals depending on the local rates of nucleation, agglomeration and crystal growth. The crystallisation time scales are orders of magnitude longer than the flow timescales. Although this tends to homogenise the crystal size and supersaturation throughout the tank, it also makes the numerical problem stiff. The precipitator under consideration was poorly mixed, with particles settling to a high concentration in the lower part of the tank. A number of cases with different feed rates and impellor speeds were investigated. It was demonstrated that they lead to different final crystal size distributions depending on residence time, supersaturation and solids concentration.

NOMENCLATURE

Roman

A	Aluminate ion concentration (kg m^{-3})
A^*	Supersaturation conc., 74.15 (kg m^{-3})
\mathbf{B}	Buoyancy force (N m^{-2})
B_u	Nucleation rate ($\text{m}^{-3} \text{s}^{-1}$)
$C_{\alpha\beta}$	Inter-phase momentum transfer coefficient ($\text{kg m}^{-3} \text{s}^{-1}$)
d	Particle diameter (m)
ΔE	Activation energy (J mol^{-1})
G	Linear growth rate (m s^{-1})
g	Supersaturation order (dimensionless)
k_a	Agglomeration rate constant
k_g	Growth rate constant
k_n	Nucleation rate constant
M	Moment of the size distribution (m^i)
m	Mass (kg)
\dot{m}	Inter-phase mass transfer rate (kg s^{-1})
N	Particle number (m^{-3})
p	Pressure (N m^{-2})
R	Ideal gas constant 8.314 ($\text{J mol}^{-1} \text{K}^{-1}$)
r	Discretisation ratio, d_{i+1}/d_i (dimensionless)
S	Source ($\text{kg m}^{-3} \text{s}^{-1}$)
T	Temperature, fixed here to 353 (K)
t	Time (s)
\mathbf{U}	Velocity (m s^{-1})
V	Particle volume (m^3)

Greek

β	Agglomeration kernel ($\text{m}^{-3} \text{s}^{-1}$)
ϕ	Volume fraction (dimensionless)
ρ	Density (kg m^{-3})
Γ	Diffusivity ($\text{kg m}^{-1} \text{s}^{-1}$)
μ	Viscosity ($\text{kg m}^{-1} \text{s}^{-1}$)
γ_{tot}	Total shear rate (s^{-1})
γ	Steady shear rate, i.e. $\frac{1}{2}(\nabla\mathbf{U}+\nabla\mathbf{U}^T)$, (s^{-1})

Subscripts

α, β	Phase (continuous or dispersed)
i, j, k	Particle size intervals

INTRODUCTION

Modelling of crystallisation processes attracts considerable attention due to the industrial importance of this separation and purification technique. Gibbsite crystallisation, for example is an important stage in the production of alumina, which is used as the feedstock for aluminium smelting. Gibbsite precipitating system has been studied by this group for more than a decade and process models of different levels of complexity have been developed. They include simple well-mixed crystallisation models as well as so-called compartmental models to describe in-homogeneously mixed crystallisers (Li *et al.*, 2003b).

Currently, methods for modelling particle/bubble size distributions as part of CFD simulations are becoming increasingly widely used (Jones *et al.* 2003; Heath & Koh, 2003; Sha *et al.* 2006; Koh & Schwarz 2006). There are two main drivers for this, firstly to account for the fact that the particle size may vary through the flow. In practice the particle/bubbles may vary both spatially and locally and this may alter both the overall flow behaviour and cause segregation based on size. The second driver is to use CFD as an environment to model the reaction kinetics of aggregation, nucleation, breakage, coalescence, growth, etc. A variety of practical systems have been modelled by this approach, for example particulate systems such as flocculation, coagulation and crystallisation, and also bubbly flows in flotation columns or solvent extraction circuits (Lane *et al.*, 2000).

Two main approaches are used to model systems with changing particle size distribution, the population balance approach, and the moment method. Both solve the reaction kernels describing the underlying physics of the rates of aggregation, growth etc, but the methods vary in their approach to solving the kernels. While the population balance method resolves a complete PSD, the moment method only gives reduced information - moments of the underlying PSD. Numerically, the population balance is solved using a discretised PBE approach, which typically

requires 20-100 size groups. Since each size group gives an additional mass or scalar transport equation, adoption of this method was previously hampered due to the computational expense.

The moments approach (Marchisio *et al.* 2006) solves instead the moments of the population balance, where the moments are given by:

$$M_i = \sum_k N_k d_k^i \quad (1)$$

Where M_i is the i^{th} moment, and N_k is the number of k^{th} sized particles with the diameter d_k . For example, the zeroth moment ($i = 0$) is the total number of particles, and the third moment is proportional to volume. A number of moments must be solved for closure, typically zero through fifth. Although this is significantly less than the number of channels required for a population balance, it may be difficult to reconstruct the complete size distribution from a limited number of moments. In some cases, however, knowing the size distribution may not be important, for example the average inter-phase drag can be calculated from the Sauter mean (ratio of the second and third moments), and the moment method may be appropriate.

This paper uses the former approach, solving the full population balance model, to investigate gibbsite crystallisation in a continuous stirred tank crystalliser. The modelling approach and implementation is described, along with a couple of case studies.

MODEL DESCRIPTION

A conventional steady-state Eulerian-Eulerian 2-phase model is used with the standard $k-\varepsilon$ turbulence model acting in the continuous phase. The phases share a common pressure field, with the momentum equations coupled via the inter-phase drag due to the liquid-particle slip. Implementation is in CFX-4, with extensive use of additional Fortran to include the population balance and extra physics.

The population balance size distribution is modelled via a series of transported scalars associated with the dispersed (particle) phase. I.e., the scalars share the velocity field with the second phase although they are diffused according to their own concentration gradients and have their own population balance source terms:

$$\begin{aligned} \frac{\partial \phi_\beta \rho_\beta N_{\beta i}}{\partial t} + \nabla \cdot [\phi_\beta \rho_\beta \mathbf{U}_\beta N_{\beta i} - \Gamma_{x,\beta} \nabla (\phi_\beta N_{\beta i})] \\ = \phi_\beta \rho_\beta S_\beta + \sum_{\beta=1}^{N_p} (\dot{m}_{\beta\alpha} N_{\beta i} - \dot{m}_{\alpha\beta} N_{\alpha i}) \end{aligned} \quad (2)$$

Where S_β is the source term from the population balance, and the final term is due to inter-phase mass transfer, which is also included to account for a significant transfer of dissolved alumina from the liquid to particle phase.

The population balance source term is comprised of contributions from nucleation, agglomeration and growth. Nucleation gives the birth rate of particles in the smallest size range (Rawlings *et al.*, 1993):

$$B_u = \frac{\partial N_1}{\partial t} = k_n \left(\sum_i N_i \right)^2 \left(\frac{A - A^*}{A^*} \right)^n \quad (3)$$

The above expression relates nucleation rate to precipitation process variables such as, total number of particles, and supersaturation.

Agglomeration is the process of cementing the crystals simultaneously with deposition of gibbsite from solution. The agglomeration rate can be modelled as a function proportional to the agglomeration kernel and product of particle numbers in aggregating size fractions. The particle size discretisation is critical to the subsequent formulation of agglomeration contribution (Hounslow *et al.*, 1988)

$$\begin{aligned} \frac{\partial N_i}{\partial t} = \sum_{j=1}^{i-2} 2^{j-i+1} \beta_{i-1,j} N_{i-1} N_j + \frac{1}{2} \beta_{i-1,i-1} N_{i-1}^2 \\ - N_i \sum_{j=1}^{i-1} 2^{j-i} \beta_{i,j} N_j - N_i \sum_{j=i}^{\infty} \beta_{i,j} N_j \end{aligned} \quad (4)$$

In the above approach the crystal size is discretised according to a geometric progression where each particle size group has double the volume of the last, ie:

$$V_i = 2V_{i-1} \quad (5)$$

Or, in terms of diameter:

$$d_i = \sqrt[3]{2} d_{i-1} \quad (6)$$

The agglomeration kernel is assumed to be size independent, and a function of the total (γ_{tot}) (steady + turbulent) shear rate and the growth rate (G):

$$\beta = k_a \gamma_{tot}^{-1.2} G \quad (7)$$

More advanced expressions for the agglomeration kernel, such as developed recently by Ilievski and Livk (2006), can also be included using the same approach. The crystal growth rate in gibbsite precipitation can be modelled as (Li *et al.* 2003a):

$$G = k_g e^{\frac{-\Delta E}{RT}} \left(\frac{A - A^*}{A^*} \right)^g \quad (8)$$

The crystal growth rate expression could be incorporated directly into the population balance (Equation 4). However, the effect the crystal growth is to convect particles up through the size ranges and can as such be treated as a convective term within the sink/source term of Equation 2. In our case, the central difference approximation was used for its accuracy and simplicity, although not surprisingly it has previously been observed to be unstable under some conditions (Hounslow *et al.*, 1988).

$$\frac{\partial N_i}{\partial t} = \frac{2G}{(1+r)d_i} \left(\frac{N(i-1)r}{r^2-1} + N(i) - \frac{N(i+1)r}{r^2-1} \right) \quad (9)$$

In addition to the population balance number density scalars (N_i), a number of additional transported scalars are used to model other variables, in particular aluminate and caustic concentrations in solution. These dissolved species determine the supersaturation in solution at a given temperature. The additional scalars have transport

equations similar to Equation 2, with the source term reflecting the inter-phase mass transfer.

The inter-phase mass transfer is sufficient to warrant inclusion into the hydrodynamic and volume fraction equations. Overall the mass transfer is given by a sum of the contributions from growth and nucleation:

$$\frac{\partial m}{\partial t} = 3 G \rho_s \frac{\pi}{6} \sum_i N_i d_i^2 + B_u \frac{\pi}{6} d_1^3 \rho_s \quad (10)$$

I.e. the volume fraction equation is:

$$\frac{\partial \rho_a \phi_a}{\partial t} + \nabla \cdot (\rho_a \phi_a \mathbf{U}_a - \Gamma_a \nabla \phi_a) = \sum_{\beta=1}^{N_p} (\dot{m}_{a\beta} - \dot{m}_{\beta a}) \quad (11)$$

with the momentum equation:

$$\begin{aligned} \frac{\partial}{\partial t} (\phi_a \rho_a \mathbf{U}_a) + \nabla \cdot (\phi_a (\rho_a \mathbf{U}_a \otimes \mathbf{U}_a - \mu_a (\nabla \mathbf{U}_a + (\mathbf{U}_a)^T))) \\ = \phi_a (\mathbf{B} - \nabla p_a) + \sum_{\beta=1}^{N_p} C_{a\beta} (\mathbf{U}_\beta - \mathbf{U}_a) \quad (12) \\ + \sum_{\beta=1}^{N_p} (\dot{m}_{a\beta} \mathbf{U}_\beta - \mathbf{U}_a \dot{m}_{\beta a}) \end{aligned}$$

Inter-phase drag is given by the Schiller and Neumann (1933) modification of Stokes' law to intermediate particle slip Reynolds' numbers

In addition, the transfer of dissolved alumina out of the continuous phase changes its density. In this work, the following equation for the liquid density was used, which describes its dependency on aluminate, caustic, and temperature:

$$\rho_\beta = 1051 + 0.992 [\text{Na}_2\text{O}] + 0.566 [\text{Al}(\text{OH})_4^-] - 0.94 (T - 273.15) \quad (13)$$

RESULTS

1-D results to check code implementation

The results are broadly divided into two parts, the first section presents results on a simplified 1-D CFD model, which served for the comparison to a transient well-mixed MATLAB model. The subsequent section describes simulation results from a full 3-D crystallizer model.

The first step in code development/debugging in the CFD environment was to simplify the CFD model back to a 1-D model to allow a direct comparison of the CFD model and MATLAB well-mixed model. To achieve this a 1-D pipe reactor model was set up in CFX-4. The "pipe" is 1600 m long hexahedral mesh with dimensions $1000 \times 1 \times 1$ nodes and symmetry planes on the sides. The cells are spaced out progressively, i.e. smaller at the beginning of the pipe where the crystallisation reactions are the fastest. A flow velocity of 0.0044 m s^{-1} was used to give a residence time of 10 hours. All diffusive terms were knocked out to give plug-flow. Gravity was switched off, and the shear rate was fixed in the PB.

Figures 1-3 compare MATLAB results with those from CFD with plug flow. Note that the MATLAB model was run as a time-marching initial-value problem, whereas the CFD is steady-state Eulerian-Eulerian. Clearly the coding and implementation is equivalent between the

models indicated by the near exact overlapping of 4 lines in each figure; two black dotted CFD lines and two solid red MATLAB lines. The CFD results are converted to time-based results by dividing the pipe length by the flow velocity.

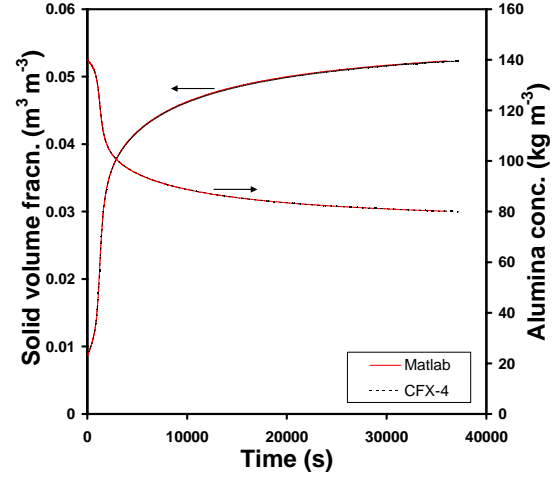


Figure 1: Comparison of CFD and MATLAB results for solid fraction and alumina concentration.

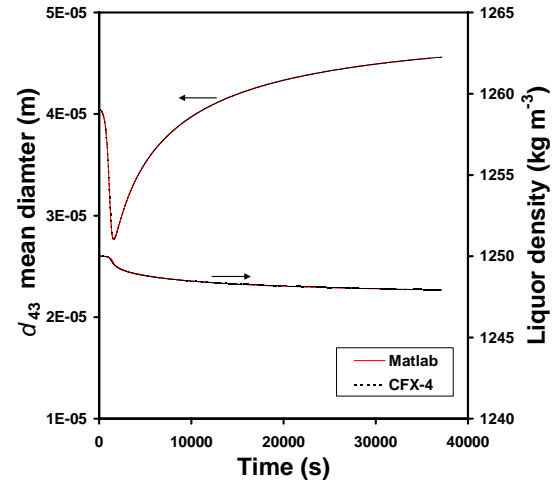


Figure 2: Comparison of CFD and MATLAB results for mean crystal size, d_{43} , and continuous phase density.

Figure 1 shows the increase in solid volume fraction due to crystallisation, and the corresponding reduction in dissolved alumina. Figure 2 shows the changes in the mean crystal size, which reduces initially from the seed crystal size due to the dominance of nucleation early in the process, followed by the growth in size later in the process when the reduced supersaturation favours agglomeration and growth. Figure 3 shows evolutions of the number of particles in different size intervals (first, fifth, tenth, etc). Again, CFD and MATLAB results are closely matched. Also notable in the plot is the wide range (y-axis) of the values of number of particles. This range contributes to the stiffness of the numerical problem since the different number densities are used together in the population balance (Equation 4).

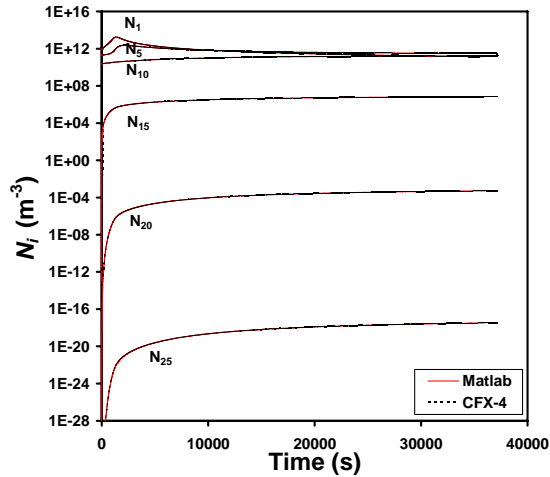


Figure 3: Comparison of CFD and MATLAB results of numbers of particles for selected size intervals.

3-D results for a continuous stirred tank crystalliser

After initial code verification the model was transferred to a continuous stirred tank crystalliser geometry. It should be noted from the outset that this model is difficult to converge satisfactorily. There are several contributing factors beyond just the number of additional transport equations being solved – and convergence is not simply a matter of patience. The model is multi-phase with the equations solved in a segregated fashion; and the liquid-phase density varies through the flow as a function of the (transported) alumina and soda concentrations. Also, the flow is inherently unstable, although running it in transient mode isn't an attractive proposition.

However, what really seems to make convergence difficult is the difference in the time-scales between the flow and crystallisation processes. The flow time-scale is in the order of seconds, as is the loop-circulation time in the lab-scale tank. However, in order to achieve the required residence time for crystallisation (hours) the velocities at the inlet and outlet patches are very low. This makes it difficult to achieve global mass, scalar, and in particular volume fraction conservation. The volume fraction matrix appears almost singular, and is quite prone to divergence or linear solver failures. Convergence strategies were along the lines of using the algebraic multi-grid (AMG) linear solver with a minimum of sweeps, no under-relaxation on the scalar, pressure or volume fraction equations, but with density heavily under-relaxed.

Due to difficulties in finding an effective convergence strategy the model is still quite simple; more advanced crystallisation kinetics will be incorporated in the future, along with heat transfer and mesh improvements. The geometry is a simple lab-scale (see Li *et al.* 2003b for details) stirred tank that is intentionally made tall-form so that it is poorly mixed with respect to solids. Particles tend to accumulating towards the base. The mesh is essentially a very simple 5 bloc hexahedral mesh of ~140 K nodes. The central block is solid, i.e. forming the impellor shaft, and the outer blocks were merged to a single block when creating the final geometry file.

There is no impellor as such, but rather a momentum source acting in a donut shaped ring in the area swept by the impellor. Downward motion and swirl are imparted

via a 2-D patch, with the velocities coded as a function of radius to generally match previous CFD simulation results (Li *et al.* 2003b), where the A310 impellor geometry was meshed directly within a sliding grid. The momentum source was implemented in user Fortran by overwriting the matrix coefficients in the momentum equations.

In addition extra turbulent kinetic energy (k) is added in the impellor patch to simulate the missing turbulence created by the impellor. This is critical for the population balance agglomeration kernel (Equation 7) which is a function of γ_{tot} , the total (turbulent + steady) shear rate, given by:

$$\gamma_{tot} = \sqrt{\frac{\varepsilon \rho}{\mu}} + \gamma \quad (14)$$

As the energy dissipation rate in our case is known from measurements, the approach taken here is to add turbulent kinetic energy until the total dissipated energy matches the desired experimental figure. Since the required k isn't known beforehand the k -source term is varied on the fly via a PID feedback loop coded in with user Fortran. I.e. k is manipulated to achieve a given ε set-point. With a little tuning of the PID coefficients this approach appears to work quite well, although it probably does little to improve convergence.

Figures 4-8 show various aspects of the baseline simulation in the continuous stirred tank crystalliser (CSTC). Figure 4 shows the overall solid volume fraction profile. This is the solver result for the dispersed phase. Note that summing the volumes of individual particle sizes gives the same result with a well-converged solution.

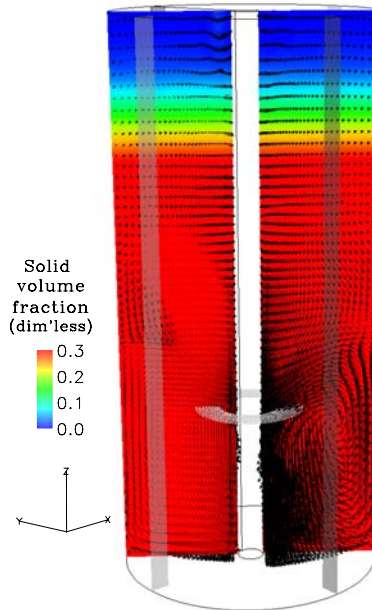


Figure 4: Solids distribution through tank. The tank is intentionally poorly mixed to encourage solid segregation and increase the hold-up.

A couple of the inlet patches are just barely visible in red at the top of the tank. The upper visible patch is the seed inlet, a minor flow in with a high concentration of seed crystals (mean size of 4×10^{-5} m). The patch below that and close to the impellor shaft is the outlet, specified as a pressure boundary in this case since there is a density change and inter-phase mass transfer. The feed inlet

(major flow in, supersaturated but free of crystals) isn't visible, but is spaced at the same height opposite from the seed inlet.

Figures 5 and 6 show the turbulent kinetic (k) and dissipated (ε) energies respectively. Note the impellor 2-D patch used to simulate the downward pumping impellor, and the resulting recirculation flow pattern in the bottom of the tank. Due to the baffles and fairly tall aspect ratio of the tank the flow is almost quiescent at the top.

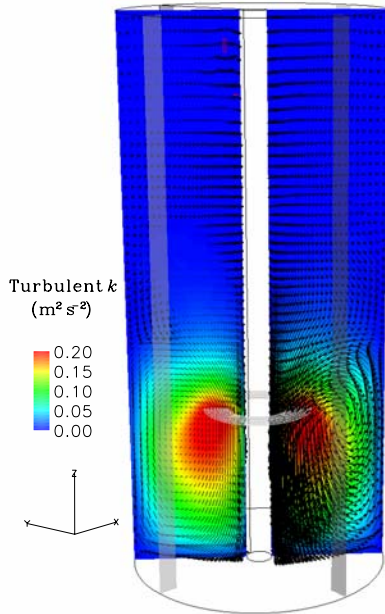


Figure 5: Turbulent kinetic energy (k), see text for details of k -source in impellor region.

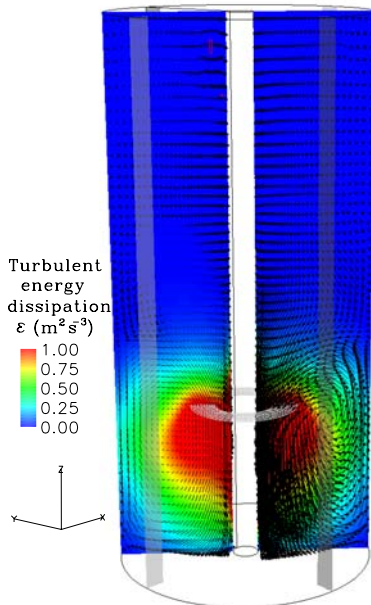


Figure 6: Turbulent dissipated energy.

Figure 7 shows the dissolved alumina concentration, which is almost perfectly mixed through the tank due to the long residence time compared to the flow time-scales. There is a slight (at an expanded scale) increase in the alumina concentration around the inlet patch towards the top of the tank. This appears to be physical rather than a

convergence issue, because a similar non-reacting scalar (not shown here) becomes completely uniform through the tank on convergence.

The final figure shows the volume weighted mean size through the tank, which is also fairly uniform apart from a small area on the top near the seed inlet, where smaller seed crystals are introduced.

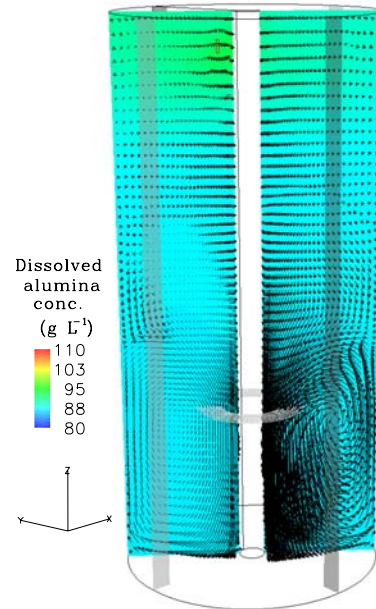


Figure 7: Dissolved alumina concentration. Due to the long residence time in the tank it is almost perfectly mixed.

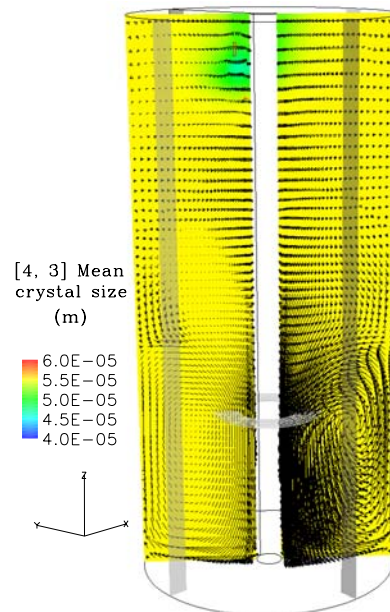


Figure 8: Mean volume weighted crystal size, d_{43} , through tank. Due to the long residence time in the tank it is almost perfectly mixed.

Comparison of CSTC runs under different conditions

Although the supersaturation and crystal size are virtually uniform throughout the tank, the shear rate and particle concentrations aren't. This impacts on the crystallisation behaviour because the crystallisation kinetics are functions of the particle number density; and in the case of

agglomeration also the shear rate. To demonstrate this a couple of additional simulations were run (figures not shown) under slightly different conditions.

The first one was run at the same seed and feed flow rates but to simulate a higher impellor rpm. Nominally the rpm was increased 30 % from 480 to 625 rpm, in this case by simplistically increasing the vertical and swirl velocities by 30 % in the 2-D “impellor” patch. From impellor power number calculations this increased the power draw ($\propto \text{rpm}^3$) and the mean energy dissipation rate ($\bar{\epsilon}$) was correspondingly increased from 0.18 to $0.40 \text{ m}^2 \text{ s}^{-3}$.

Increasing the impellor speed has a number of effects on the flow and crystallisation process. Firstly it tends to homogenise the solids in the tank by increasing both the pumping rate (i.e. convection) and turbulent diffusion. This in turn lowers the mean solids in the tank. I.e., since this is a steady-state simulation, the solids concentration builds up in the bottom of the tank until the concentration at the outlet leads to a balance with the feed solid plus mass increase due to crystallisation. So speeding up the impellor stirs up the solids in the bottom of the tank and lifts them up towards the outlet, reducing the average steady-state solids content in the tank. This in turn impacts on the crystallisation process since the crystallisation kinetics are functions of the particle number density. Reducing the solids concentration in the tank also reduces the residence time for crystals to grow. In addition, since the particle number density is lower there is less particle surface area for alumina precipitation, so the supersaturation is also increased, which then feeds back to change the precipitation kinetics. These various couplings contribute to the convergence difficulties since although the physics is coupled the equations are solved in a segregated fashion.

The final simulation discussed here was run with the original impellor speed but decreased residence time, achieved by fivefold increase of the seed and feed flow rates. As shown in Table 1, this has the overall effect of dramatically decreasing the final crystal size. The reason appears to be partly in the reduction of crystal residence time (allowing less time for agglomeration and growth) and partly because the supersaturation was higher, favouring nucleation.

	Baseline	Higher impellor rpm	Higher throughput
Mean solid fraction (dim'less)	0.23	0.09	0.193
Solid fraction at outlet (dim'less)	0.080	0.079	0.074
[4, 3] mean crystal size (m)	5.5×10^{-5}	4.4×10^{-5}	4.3×10^{-5}
Mean alumina conc. (g L^{-1})	88	92	94
Mean dissipation rate, ϵ ($\text{m}^2 \text{ s}^{-3}$)	0.18	0.40	0.18
Superficial mean residence time (s)	1.3×10^4	1.3×10^4	2.6×10^3
Liquid mean residence time (s)	1.0×10^4	1.2×10^4	2.3×10^3
Solids mean residence time (s)	4.0×10^4	2.3×10^4	8.1×10^3

Table 1: Simulation results from CSTC runs

CONCLUSIONS

A coupled population balance and CFD model for gibbsite crystallisation has been coded into CFX-4. The model is Eulerian-Eulerian 2-phase with 35 additional solid-phase scalar transport equations for the particle size intervals, and additional liquid-phase transport equations for dissolved alumina and caustic. Crystallisation

kinetics, such as nucleation, crystal growth and agglomeration are described by rate expressions containing main process variables.

Simulation results in a poorly-mixed CSTC showed that although the solids were poorly distributed through the tank the crystal size and supersaturation were relatively uniform due to the relatively long residence time compared to the flow time-scale. This difference in time-scales also contributed to the model stiffness although convergence was still achievable with the correct model set-up.

The model development is in its early stage, requiring additional developments in several areas, e.g. more complex crystallisation kinetics, the mesh density, impellor geometry and also the inclusion of appropriate enthalpy equation. However, the simulations conducted so far show that a model based on this approach is feasible and has the potential to capture complex behaviour observed in industrial crystallisers. This can be very valuable for advancing crystallisation equipment design and process optimisation.

ACKNOWLEDGEMENTS

This research was supported by the Australian Government's Co-operative Research Centre (CRC) program via the Parker Cooperative Research Centre for Integrated Hydrometallurgical Solutions.

REFERENCES

- HEATH, A.R. AND KOH, P.T.L. 2003, 'Combined Population Balance and CFD Modelling of Particle Aggregation by Polymeric Flocculant', *Third International Conference on CFD in the Mineral and Process Industries*, CSIRO, Melbourne, Australia, 10-12 December, pp. 339-344.
- HOUNSLOW, M.J., RYALL, R.L. AND MARSHALL, V.R. 1988, 'A discretized population balance for nucleation, growth and aggregation', *AIChE Journal*, Vol. 34, No. 11, pp. 1821-1832.
- ILIEVSKI, D., AND LIVK, I., 2006, 'An Agglomeration Efficiency Model for Gibbsite Precipitation in a Turbulently Stirred Vessel', *Chem. Eng. Sci.*, 61(6), 2010-2022
- JONES, I.P., GUILBERT, P.W., OWENS, M.P., HAMILL, I.S., MONTAVON, C.A., PENROSE, J.M.T. AND PRAST, B. 2003, 'The use of Coupled Solvers for Complex Multi-Phase and Reacting Flows', *Third International Conference on CFD in the Mineral and Process Industries*, CSIRO, Melbourne, Australia, 10-12 December, pp. 13-19.
- KOH, P.T.L AND SCHWARZ, M.P. 2006, 'CFD Modelling of Bubble-Particle Attachments in Flotation Cells', *Minerals Engineering*, Vol. 19, pp. 619-626.
- LANE, G.L., SCHWARZ M.P., AND EVANS, G.M. 2000, 'Modelling of the Interaction between Gas and Liquid in Stirred Vessels', *10th European Conference on Mixing* (H.E.A. van Akker and J.J. Derksen editors), Elsevier Science.

LI, T.S., LIVK, I., AND ILIEVSKI, D. 2003a, 'Supersaturation and Temperature Dependency of Gibbsite Growth in Laminar and Turbulent Flows', *Journal of Crystal Growth*, Vol. 258, pp. 409-419.

LI, T.S., LIVK, I., LANE, G. AND ILIEVSKI, D. 2003B, 'Dynamic Compartmental Models of Uniformly-Mixed and Inhomogeneously-mixed Gibbsite Crystallizers', *Chem. Eng. Technol.*, Vol. 26, No. 3, pp. 369-376.

MARCHISIO, D.L., SOOS, M., SEFCIK, J., MORBIDELLI, M., BARRESI, A. AND BALDI, G. 2006, 'Effece of Fluid Dynamic on Particle Size Distribution in Particulate Processes', *Chem. Eng. Technol.* Vol. 29, No. 2, pp. 191-199.

RAWLINGS, J.B.; MILLER, S.M.; WITKOWSKI, W.R. 1993, 'Model Identification and Control of Solution Crystallisation Processes: A review', *Industrial Engineering and Chemistry Research*, 32, 1275-1296.

SCHILLER, L. AND NAUMANN, Z. 1933 'A Drag Coefficient Correlation' *Z. Ver. Deutsch. Ing.*, Vol. 77, pp. 318-320.

SHA, A., LAARI, A. AND TURUNEN, I. 2006, 'Multi-Phase-Multi-Size-Group Model for the Inclusion of Population Balances into the CFD Simulation of Gas-Liquid Bubbly Flows', *Chem. Eng. Technol.* Vol. 29, No. 5, pp. 550-559.